Results in Engineering 29 (2026) 108817

Contents lists available at ScienceDirect

Results in Engineering

journal homepage: www.sciencedirect.com/journal/results-in-engineering

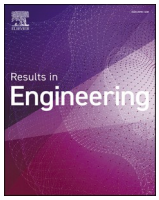

Introduction of dimensionless parameters for in-silico washout evaluation within membrane oxygenators

Jan Heyer [*], Sebastian V. Jansen, Ulrich Steinseifer, Felix Hesselmann [1], Michael Neidlin [1]

Cardiovascular Engineering, Applied Medical Engineering, RWTH Aachen University, Germany

A R T I C L E I N F O

Keywords:
Extra corporeal membrane oxygenators
ECLS
Oxygenator washout

A B S T R A C T

Extracorporeal membrane oxygenators are a key component within extracorporeal life support systems. A major complication is thrombus formation which has life-threatening consequences for the patients. The flow path within the oxygenators is a driver of thrombotic events and its optimization is a central engineering requirement, however there is a lack of quantitative metrics to assess the thrombus risk in those devices. In this study, we present an in-silico method for evaluating oxygenators' flow path and introduce quantitative metrics for the optimization of such through three dimensionless parameters defining stagnation areas, flow homogeneity, and washout capabilities. Based on these parameters, we compare four commercially available oxygenators with respect to their thrombus risk at flows between 0.5–1.5 l/min and flow pulsatilities between 25–75 %. The results outline how overall oxygenator design - wound vs. stacked fiber bundles – impacts washout metrics. Further on, we uncover that while low flow pulsatility of 25 % does improve washout, further increase does not yield any additional benefit. This work shows the suitability of the presented parameters for a computational evaluation and optimization of existing or newly developed oxygenators.

1. Introduction

Extracorporeal life support systems (ECLS) provide blood oxygenation, decarboxylation, and circulatory support through blood pumps and membrane oxygenators. They are used in the intensive care unit for patients with severe respiratory and cardiac failure. Gas exchange is achieved by directing blood through a densely packed bundle of hollow fiber membranes, while sweep gas flows through the inner fiber lumina [1]. A major complication of oxygenators during ECLS therapy is intra-device thrombosis with an incidence of approximately 20–30 % [2–4]. Thrombotic events decrease gas transfer and increase flow resistance of the fiber bundle, ultimately leading to mechanical failure and the requirement of oxygenator exchanges. These exchanges increase the risk for life-threatening complications such as bleeding, embolisms, and infections [5]. An approach for thrombosis reduction without anticoagulation adjustment [6] and gas transfer performance optimization [7] lies in an optimal blood flow path through the oxygenator.

The blood flow path within an oxygenator is determined by the housing, including inlet and outlet positions, the potting margins, and the fiber bundle configurations [6,8–10]. Variations in inlet and outlet placement lead to different flow distributions, which may generate regions of recirculation and flow inhomogeneity. Such areas are known promoters of thrombosis [6]. With respect to the fiber bundle, clinically used oxygenators generally have two different fiber bundle settings - stacked fiber mats or fiber mats that are wound around a core. Both fiber bundle configurations differ in fiber orientation in relation to blood flow direction, resulting in different hydraulic resistances. In stacked oxygenators, the fibers are orientated orthogonally to the blood flow, while in most of the wound oxygenators, the blood flows predominantly along the fiber mats.

In addition to oxygenator housing design and fiber bundle configuration, the flow path is influenced by flow conditions, which vary depending on the targeted therapy and patient population. In general, there are two different clinical settings for oxygenators - pulsatile and continuous flow. Overall, continuous flow is more commonly used in extracorporeal membrane oxygenation (ECMO) [11]. However, especially for neonates and children, pulsatile flow induced by roller pumps is utilized and has lower mortality due to advantages in ECMO performance for example of hemolysis and renal outcome [12–14]. In addition, no clear recommendation exists regarding the superiority of one

* Corresponding author.
E-mail address: jan.heyer@rwth-aachen.de (J. Heyer).
[1] equal contribution

https://doi.org/10.1016/j.rineng.2025.108817
Received 8 September 2025; Received in revised form 5 December 2025; Accepted 18 December 2025
Available online 19 December 2025

flow mode over the other in terms of oxygenator performance [15]. Beyond that, it remains vastly unexplored how pulsatile flow affects the washout of oxygenators.

The blood flow paths and their washout behavior are generally investigated in the literature in flow simulation studies to determine the flow characteristics of specific oxygenators [9,10], compare inlet and outlet designs [6,8] and assess fiber bundle configurations [7,16]. Various methods are used to evaluate different washout parameters, like velocity fields, volume residuals and inhomogeneities in flow distribution [6,8–10]. However, these individual methods lack a standardized definition as a baseline for a dimensionless comparison. Due to the absence of such an in-silico definition, comparisons of flow distributions within oxygenators are challenging to perform in detail and translation of findings between individual studies remains limited. Currently, time and cost-consuming experiments resulting only in qualitative insights or retrospective studies are required to define potential areas within oxygenators where the risk of thrombotic events is increased due to unfavorable flow distributions [17–19].

In consequence, establishing a computational framework for washout analysis represents a key opportunity to better identify high-risk regions for thrombosis and to guide future oxygenator design and optimization. In this study, we introduce three dimensionless parameters to describe the washout behavior of oxygenators using computational fluid dynamics (CFD) simulations. These dimensionless parameters enable a direct comparison of oxygenators independent from size and therapy to evaluate the differences in washout behavior and flow path design. We showcase the use of those parameters to investigate the influence of pulsatile and steady flow conditions within four commercially available oxygenators.

2. Methods

Four clinical oxygenators were chosen for the numerical flow simulations within this study. The oxygenators Quadrox Small Adult (QSA) (Getinge Cardiopulmonary GmbH, Rastatt, Germany), ILA, Hilite 800 and Hilite 2400 (Fresenius, Stolberg, Germany) were selected and reverse-engineered to generate the necessary CAD Data using Creo (PTC Inc. Boston, Massachusetts, United States). The Quadrox and ILA, are both examples for stacked, rectangular shaped oxygenators. Both have a similar design of the fiber bundle and the inlets and outlets are placed opposite of each other in the same corner of the housing with distributor plates placed in series. In contrast to the ILA with only one fiber bundle, the Quadrox consists of two fiber bundles in series, of which one is additionally used for heat exchange, separated by a distributor plate. The upstream bundle consists of gas exchange membranes interspersed with heat exchange capillaries, while the second consists solely of gas exchange fiber mats. The ILA consists of only one fiber bundle compartment. The two Hilite oxygenators consist of wound fiber bundles and are predominantly used for cardiopulmonary bypass and long-term applications. Blood in these oxygenators flows through two fiber compartments: The first compartment incorporates heat exchange capillaries and the second hollow fibers for gas transfer.

2.1. CFD model – washout

The fiber bundle was modeled as a porous medium as state-of-the-art technique to simulate the flow in such complex geometry at reasonable computational resources. Porosity was calculated according to the measured fiber count and diameter using microscopy within the corresponding fiber bundles. Permeability was calculated according to Darcy's Law based on the Ergun equation for theoretical viscous and kinematic pressure losses. The viscous and kinematic losses were calculated and combined to a total theoretical pressure loss based on the given and measured information about the fiber and bundle geometry, volume flow, and blood properties. The properties and permeabilities are provided in Supplementary Material 1. The fluid domains were meshed using ANSYS Meshing 2021 (ANSYS Inc., Canonsburg, PA, USA). The meshes of all oxygenators were progressively refined until independence was reached, with pressure drop across the oxygenator and cross-sectional flow fields within the fiber bundle as evaluation criteria. Independence was achieved at element sizes of 4×10^{-4} m for Hilite 800 and of 5×10^{-4} m for both the Hilite 2400 and ILA. For the QSA, the mesh was divided into two porous domains with an element size 5×10^{-4} m and fluid domains with an element size of 4×10^{-4} m. Full mesh specifications are shown in Supplementary Material 1. Blood was modeled as healthy human blood at 37 °C with shear-dependent viscosity, using the model by Ballyk et al. [20]. Flow was considered laminar with Re < 50 [9,21]. The inlet boundary condition was defined as a mass flow inlet with the inflow rate defined according to Eq. (1), where $\dot{Q}$ in L/min is the mean volume flow rate, $\dot{Q}_{AMP}$ in L/min is the volume flow amplitude and BPM in 1/min is the frequency of pulsation.

$$Inflow = \dot{Q} + \dot{Q}_{AMP} \times \sin\left(2 \times \pi \times \frac{BPM}{60} \times t\right) \quad (1)$$

The outlet boundary condition was set as opening with a relative pressure of 101.325 Pa. Convergence was achieved at a root mean square error threshold of 10^{-4}. All simulations were performed in two steps. First, a steady-state simulation was run to initialize the system with blood (fluid 1 - "blood old") filling the oxygenator. The result from the steady state simulation served as initialization to a transient simulation, in which entering blood (fluid 2 - "blood new"), modeled as a second phase with the same properties, displaced the initial fluid. The initial volume fraction at the inlet boundary was set to 1 for "blood old" to and to 0 for "blood new" to for the steady state and to 0 for "blood old" and 1 for "blood new" for the transient simulation. The fluid and porous domains were all initialized with "blood old" set to 1 for the steady state simulations. Interphase transfer was modeled as a mixture model with a 1 mm interface length scale and a momentum transfer with a drag parameter of 0.44. Timesteps (Δt_s) for the transient simulation were set to 0.05 s. The total simulation runtime (T) was set to twice the theoretical washout time, a conservative estimate to achieve a realistic washout and a complete periodic cycle under pulsatile flow conditions. The theoretical washout time was calculated using the oxygenator's volume divided by the given volume flow. All simulations were performed in Ansys CFX 21R2 on an 18 core 2.4 GHz Intel Xeon E5–2640 CPUs and 64 GB RAM. The oxygenators were analyzed according to the three different dimensionless parameters described below. Three different volume flow rates ($\dot{Q}$) 0.5, 1.0 and 1.5 L/min, each with different amplitudes of 0, 25, 50 and 75 %, without and with a pulse of 60 bpm were simulated. The effects of flow settings, fiber bundle configurations and oxygenator designs were compared based on the defined parameters. The velocity distribution from the CFD porous medium model for an upscaled stacked oxygenator has been compared to experimental particle imaging velocimetry measurements in our prior work performed by Kaesler et al. [22], overall showing good agreement between numerical and experimental results.

Three dimensionless parameters with a range from 0 to 1 for stagnation areas ($W_{Stagnation}$), homogenous and rapid washout ($W_{Washout}$) and homogeneous flow distribution ($W_{Homogeneity}$) were defined to evaluate and compare the simulated oxygenators in their washout behavior.

2.2. Stagnation areas

The stagnation areas are derived from transient velocities. The stagnation index (SI) is defined in Eq. (2), with a critical stagnation area SI_{crit} set to a velocity v_{crit} of 1 mm/s. The critical velocity was selected from the study by Liao et al. [23] who investigated blood stagnation risk in the left ventricle during cannulation with a left ventricular assist device. A stagnation volume (V_{stagn}) is determined for fluid volume (V_i) with $SI_i < SI_{crit}$ (Eq. (3)). The dimensionless parameter $W_{Stagnation}$ is the

stagnation volume divided by the total priming volume of the oxygenator (V_{PV}) (Eq. (4)).

$$SI_i = \frac{\int_0^T v_i(x, y, z, t)dt}{T} \quad (2)$$

$$V_{stagn} = \sum V_i(SI_i) \quad (3)$$

$$W_{Stagnation} = \frac{V_{stagn}}{V_{PV}} \quad (4)$$

2.3. Rapid and effective washout

The effectiveness of washout $W_{Washout}$ is evaluated based on the residual volume of initial fluid (fluid 2 – "blood old") within the oxygenator at total time T. During the simulation, the initial old blood volume (V_{BO}) is progressively displaced by the incoming new blood volume. The dimensionless parameter $W_{Washout}$ as described in Eq (5). is quantified as the cumulative remaining volume V_{BO} at total time T relative to the total priming volume of the oxygenator V_{PV}:

$$W_{Washout} = \frac{V_{BO}(T)}{V_{PV}} \quad (5)$$

The smaller the parameter $W_{Washout}$, the more effective is the washout.

2.4. Homogeneous flow distribution

The homogeneous flow distribution provides the spatiotemporal variation of velocities in the fiber bundle. First, the local standard deviation of velocities ($v(t)_{Lstd}$) based on the number of timesteps (n) and theoretical mean velocities ($v(t)_{\mu}$) are calculated (Eq. (6) & (7)) based on all cross-sections (A_i) perpendicular to the flow direction through the fiber bundle. The velocities are used to compute T_{rel}, which describes time-related degree of irregularity of the velocity behavior for each time step (t_s) (Eq. (8)). The dimensionless parameter $W_{Homogeneity}$ uses this integral of relative differences in velocity to define and evaluate the relative flow distribution, the smaller the parameter $W_{Homogeneity}$ the more homogeneous is the flow (Eq. (9)).

$$v(t)_{Lstd} = \sqrt{\frac{1}{n}\sum_i \left(v_{\mu}(t) - v(x_i, y_i, t)\right)^2} \quad (6)$$

$$v_{\mu}(t) = \frac{\dot{V}(t)}{A_i} \quad (7)$$

$$T_{rel} = \int_0^T \frac{v(t)_{Lstd}}{v(t)_{\mu}} dt_s \quad (8)$$

$$W_{Homogeneity} = \frac{T_{rel}}{T} \quad (9)$$

2.5. Verification experiment

To verify the simulations, a simplified in vitro experiment was conducted. The experiment was performed using clear and colored water-glycerol fluid adjusted to a viscosity of 3.7 mPas, equal to blood at 37 °C. The test circuit, illustrated in the supplementary materials 2, consists of two reservoirs (clear and dye fluid), two rotary blood pumps, four valves (V_{1-4}), flow and pressure measurement points (p_1, p_2, Q), light-absorption measurement points (C_1, C_2), and a test object. The experiment was divided into four phases: regular operation, injection phase, test phase, and back to regular operation. The valves and pumps were programmed to maintain continuous flow throughout the experiment and switch between the reservoirs. During regular operation, the valves of the clear fluid reservoir (V_1 and V_3) were open. At the start of the injection phase, the valves switched to the dye reservoir (V_2 and V_4 open) to deliver a fluid bolus for 4 s. After 4 s, the valves were switched to test phase (V_1 and V_4 open). During the test phase the time of bolus washout was measured. The measurement started as soon as the pre-test object light absorption (C_1) measurement detects the bolus and ended when the post-test object light absorption (C_2) measurement stopped recognizing the bolus. This time was defined as $T_{99,exp}$. Finally, the valves switched back to regular operation (V_1 and V_3 open). All simulated oxygenators were tested within the circuit at a continuous volume flow of 0.5, 1, and 1.5 L/min. The measured time was used to compare with the time to 99 % washout of 'blood old' during the CFD simulation.

2.6. Statistical analysis

The different oxygenators were compared regarding the dimensionless numbers. In addition, the effect of pulsatility and flow rate on the washout performance was assessed. All statistical comparisons were performed with the Kruskal-Wallis test and Dunn's post hoc test with 0.05 as the significance threshold. R-Studio was used for all statistical analyses.

3. Results

The resulting flow distribution is shown in Fig. 1 at a volume flow of 1 L/min with a pulsatility index (PI) of 75 % at the related total time T. The flow distribution is illustrated by the velocity through the oxygenator.

The wound and stacked oxygenators show different velocities, with a relatively slower velocity through the stacked fiber bundles (Fig. 1, lower subpanels) compared to the wound ones (Fig. 1, upper subpanels). Overall, the velocity in each oxygenator slows down homogenously from the inlet to the fiber bundle and has a homogeneous distribution within the bundle, while increasing again towards the outlet.

Fig. 2 shows an example of one washout simulation at different time steps of the QSA at 1 L/min flow, 60 bpm and 25 % pulsatility. The initial fluid (fluid 1 - "old blood") is shown in blue and the "new blood" in red. An inhomogeneous distribution of the blood is observable in timesteps 2 (t = 1.15 s) and 3 (t = 2.65 s), that results in stagnation regions at the corners of the fiber bundle in timestep 4 (t = 3.75 s).

3.1. Influence of oxygenator design on washout performance

The herein presented parameters are used to compare the simulated oxygenators' washout performance within the defined flow and pulsatility ranges. Fig. 3 shows the calculated parameters for the different oxygenator models.

The oxygenators present significant differences in $W_{Washout}$ and $W_{Homogeneity}$ and minor differences in $W_{Stagnation}$. The outliers in each boxplot correspond to the constant flow scenarios with 0 % pulsatility. Looking at $W_{Washout}$, all oxygenators performed significantly different. The Hilite 2400 has the lowest median value and the largest variation for different operating points. Hilite 800 and QSA are within the same range, with a slightly lower median value for Hilite800. The ILA has the highest median value. Two significant differences are observed for the second parameter $W_{Stagnation}$ between the two Hilite oxygenators and between Hilite 800 and ILA. The median values of the oxygenators are all in close range. The critical stagnation volume (green) of $W_{stagnation}$ is additionally illustrated for the four oxygenators in Fig. 4 at a volume flow of 1 L/min and a pulsatility index of 75 % as an example of the parameter's visual result.

The third parameter $W_{Homogeneity}$ shows again significant differences between the oxygenators, except between ILA and QSA. Hilite 2400 has the highest median, followed by Hilite800, ILA, and QSA, which has the lowest median. The Hilite oxygenators exhibit a smaller spread (distance between 25th to 75th percentile) than the ILA and QSA oxygenator. A

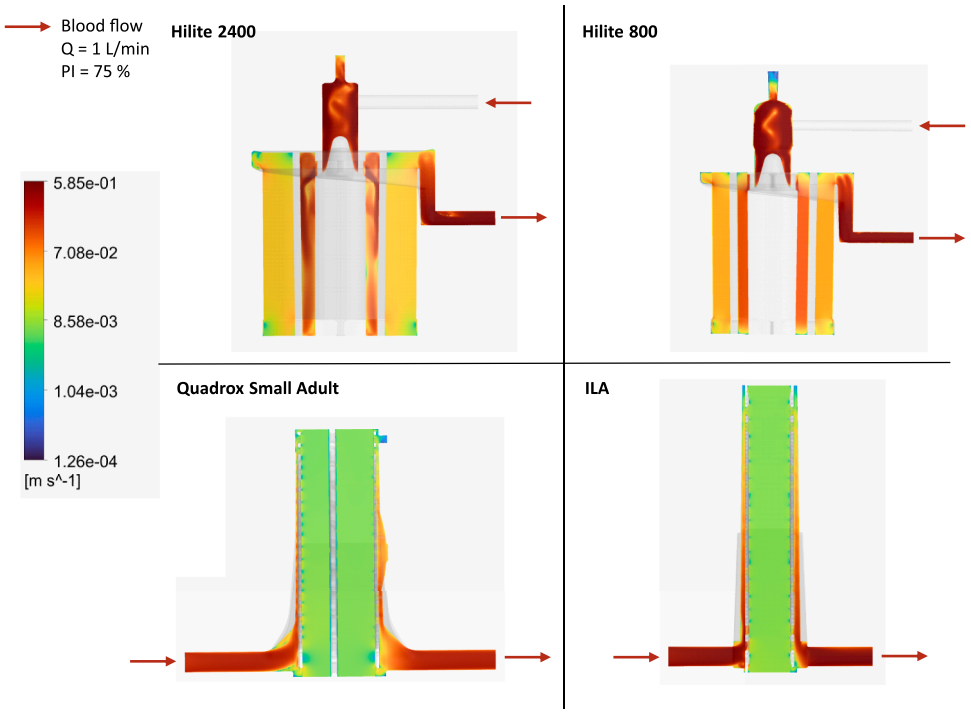

Fig. 1. Flow distribution within the wound oxygenators (Hilite 2400 top-left, Hilite 800 top right) and stacked oxygenators (QSA bottom-left and ILA bottom-right).

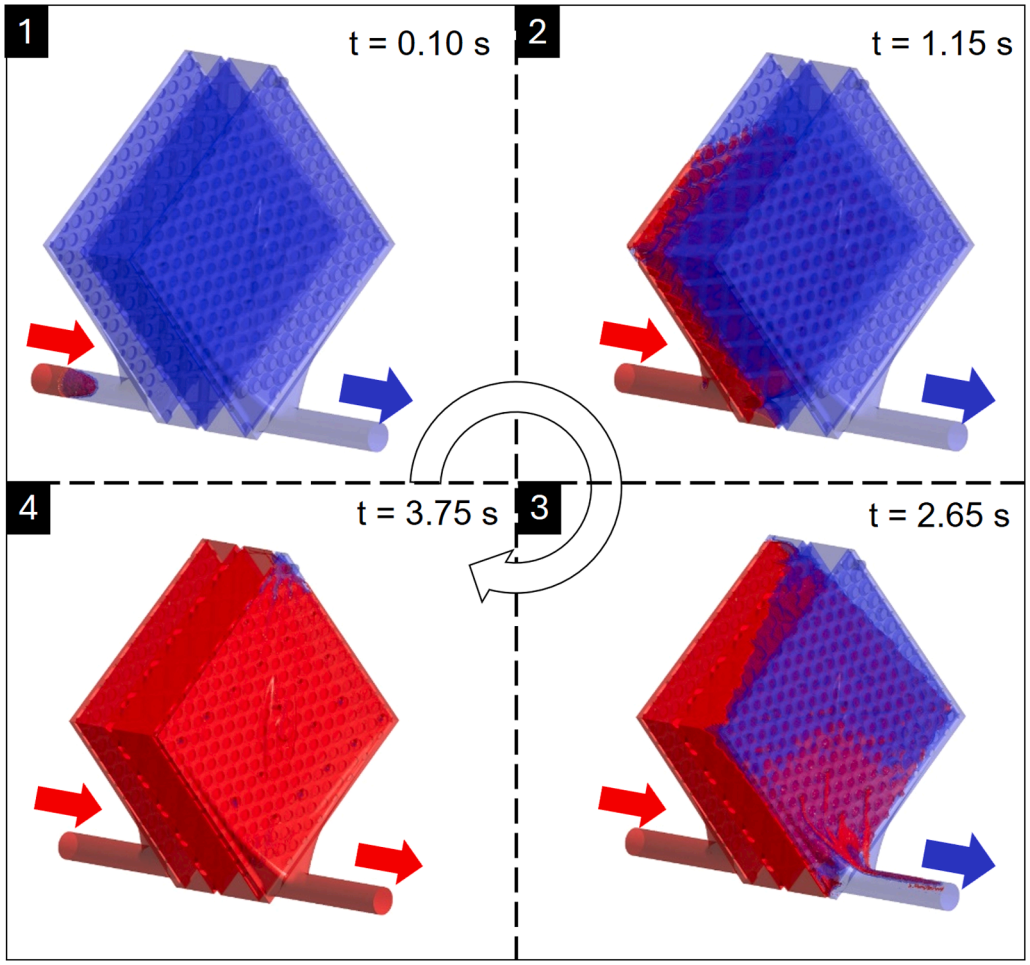

Fig. 2. Washout in the QSA oxygenator at timesteps: 0.1 s (1), 1.15 s (2), 2.65 s (3) and 3.75 s (4) at 1 L/min, old blood in blue and new blood in red.

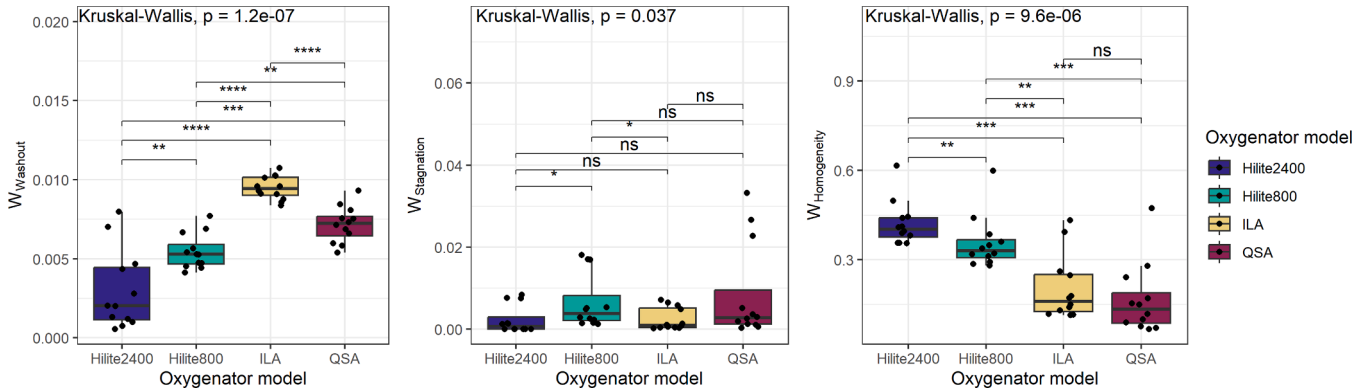

Fig. 3. The different parameters for the four oxygenator (Hilite2400 in blue, Hilite800 in green, IlLA in brown, QSA in purple) and their performance in the three washout parameters at the given operational points; ns $p > 0.5$, * $p \leq 0.5$, ** $p \leq 0.01$, *** $p \leq 0.001$, **** $p \leq 0.0001$.

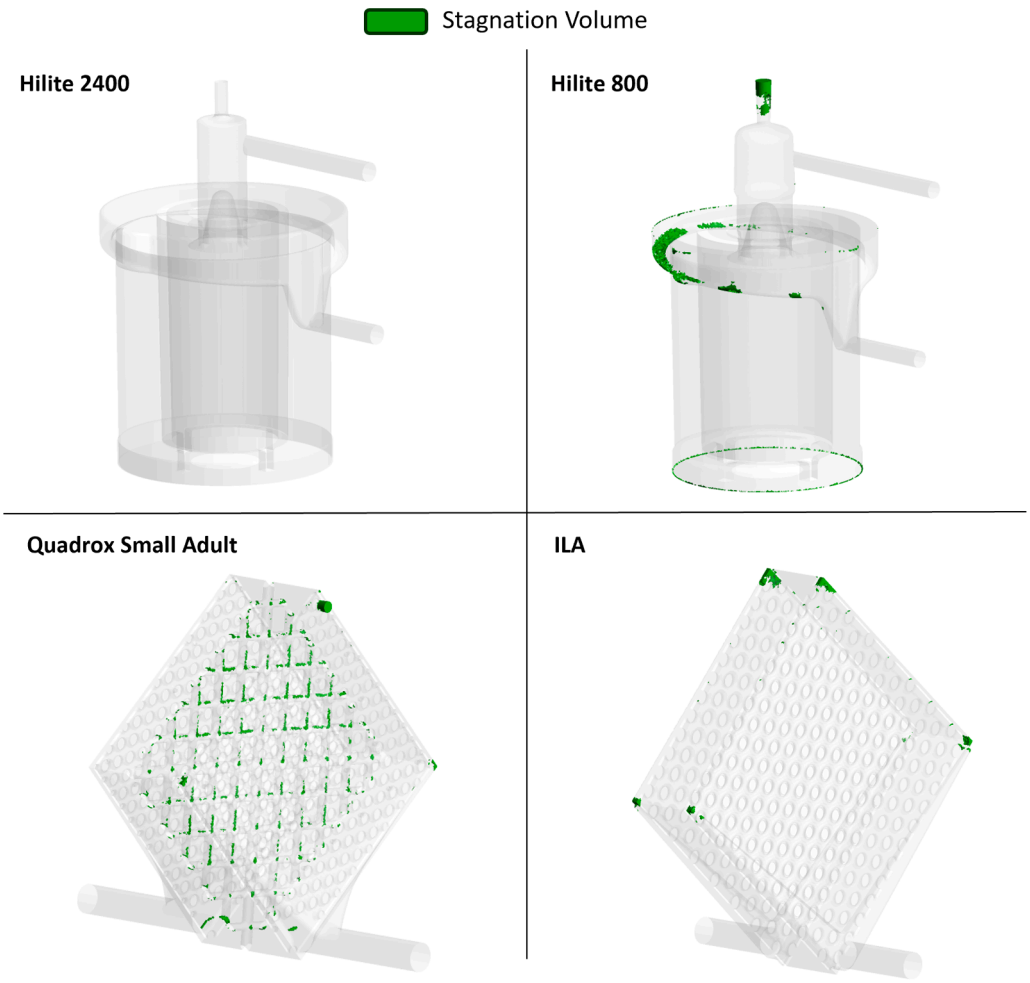

Fig. 4. Stagnation volume V_{stagn} illustrated as green volume at 1 L/min and pulsatility index of 75 %, within the wound oxygenators (Hilite 2400 top-left, Hilite 800 top right) and stacked oxygenators (QSA bottom-left and ILA bottom-right).

pairwise visualization of the parameters is shown in Fig. 5.

The relation between the parameters $W_{Washout}$ and $W_{Homogeneity}$ shows a clustering of the different oxygenators. An inverse relation between $W_{Homogeneity}$ and $W_{Washout}$ is observable with an optimum in the lower left corner of the plot. The relation between $W_{Washout}$ and $W_{Stagnation}$ also shows clustering. The final relation between $W_{Homogeneity}$ and $W_{Stagnation}$ does not show a clustering of the different oxygenators.

3.2. Influence of pulsatility on washout performance

The parameters concerning the tested pulsatility are shown in Fig. 6 for each oxygenator.

The parameter $W_{Washout}$ does not show a significant difference in pulsatility, but a decrease of $W_{Washout}$ for each oxygenator by increasing pulsatility can be recognized. $W_{Stagnation}$ shows a significant difference for constant flow and all three pulsatility levels. There is no significant difference between each of the pulsatilities. $W_{Homogeneity}$ shows an

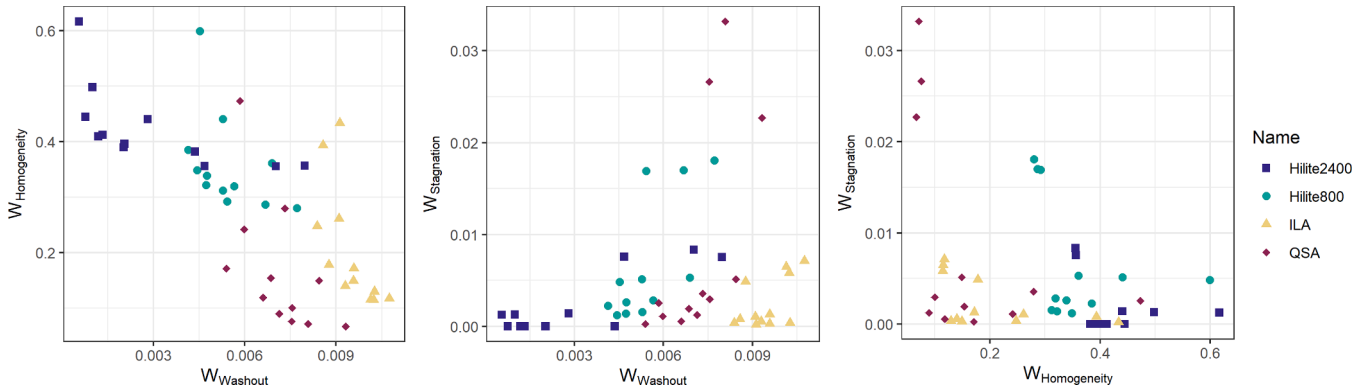

Fig. 5. Relation between the different washout parameters (Hilite2400 in blue, Hilite800 in green, IlLA in brown, QSA in purple).

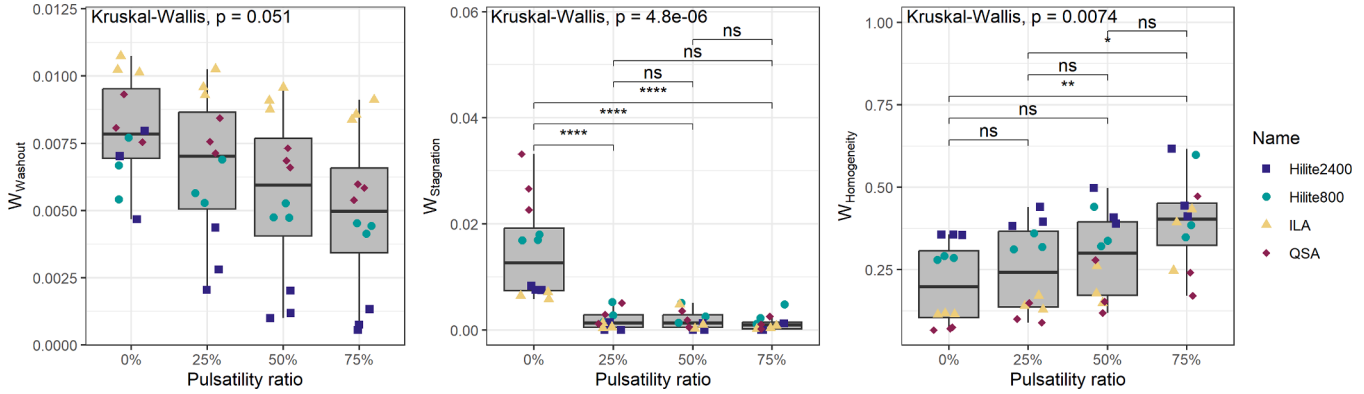

Fig. 6. Washout parameters depending on the different pulsatility ratios (Hilite2400 in blue, Hilite800 in green, IlLA in brown, QSA in purple); ns $p > 0.5$, * $p \leq 0.5$, ** $p \leq 0.01$, *** $p \leq 0.001$, **** $p \leq 0.0001$.

increase in inhomogeneity with an increase in pulsatility, with a significant difference for a pulsatility of 75 % compared to constant flow or 25 % pulsatility.

3.3. Influence of net flow rate on washout performance

The parameters depending on the different volume flows are shown in Fig. 7.

No significant differences regarding flow were found among all parameters. For $W_{Stagnation}$, the outlier design points represent the operating conditions without pulsatility.

3.4. Verification experiment

The resulting washout times from the verification experiment and simulations are shown in Table 1, aligned with the set volume flows. In addition, the proportional differences between the two times were calculated and are shown in the table. A mean difference between experiment and simulation of 9.5 % is observed. For the simulation of ILA, 99 % of blood old washout was not reached during the predefined simulation time; the time within Table 1 was reported as the total simulation time, and no proportional difference was calculated.

4. Discussion

The presented study introduced three dimensionless parameters to

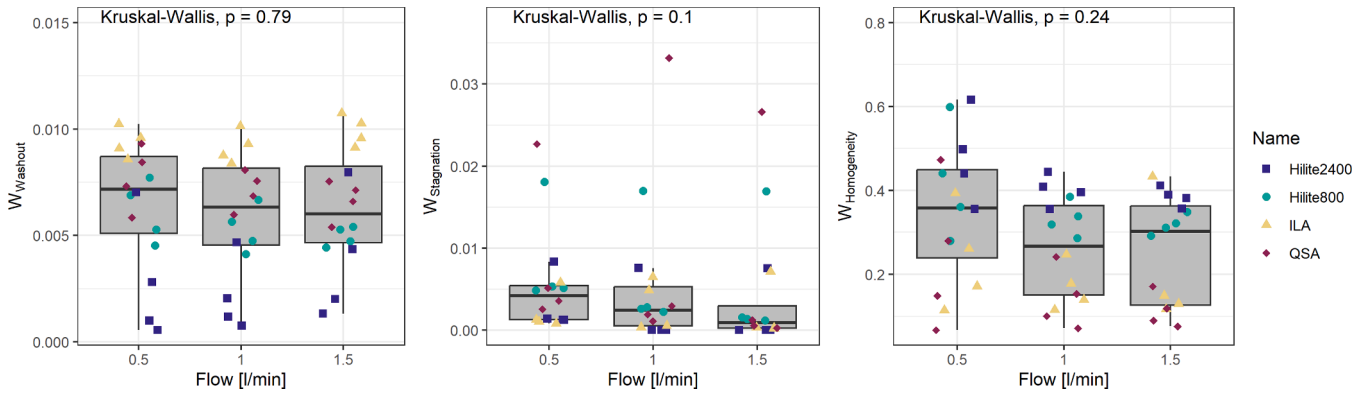

Fig. 7. Washout parameters depending on the three different flow rates (Hilite2400 in blue, Hilite800 in green, lLA in brown, QSA in purple).

Table 1
Measured and simulated washout time of blood old. *extrapolated due to measurement error., ** time at 98.7 % washout, *** time at 98.8 % washout.

Oxygenator	Volume flow in L/min	Measured time in s	Simulated time in s	Time difference in %
QSA	0.5	35.6	38.5	7.5
	1	17.4	18.0	3.3
	1.5	12.3	11.7	5.1
ILA	0.5	32.0	38.5**	-
	1	15.3	19.2***	-
	1.5	10.8	12.8**	-
Hilite2400	0.5	22.6	24.5	7.8
	1	11.3	12.8	11.7
	1.5	9.0*	10.1	10.9
Hilite800	0.5	12.1	13.4	9.7
	1	7.5	6.5	15.3
	1.5	4.7	4.1	14.6

evaluate the washout behavior of full-scale oxygenators in silico. Unlike previous models that focused on isolated components, such as inlets or outlets [6,8], the presented method enables full-path flow tracing and dimensionless comparison across different devices. Such information can support the design of oxygenators that are less susceptible to flow-induced thrombus formation.

Similar approaches have been chosen for other applications, such as identifying thrombus risk regions in left ventricular device inflow cannulation sites by calculating the pulsatility index of the intraventricular flow field and instantaneous stagnation regions [23]. Further on, stagnation regions in rotary [24] and pulsatile [25] blood pumps were determined through CFD washout simulations. However, these earlier approaches did not provide a framework for quantitative comparison across devices or flow patterns. The dimensionless parameters introduced herein address this gap and enable direct comparison, as demonstrated by four commercially available oxygenators.

The combination of $W_{Washout}$ and $W_{Homogeneity}$ delivered significant differences among the oxygenators, with an inverse relationship between the two parameters (Fig. 5). Investigating $W_{Washout}$ and $W_{Homogeneity}$ opens up the potential for a Pareto-based optimization to balance flow homogeneity and risk of blood stagnation. Overall, both parameters enable an adequate comparison between oxygenator models to evaluate the optimal geometry or operation point regarding the flow path and washout behavior. In contrast, the parameter $W_{Stagnation}$ showed almost no significant differences between the oxygenators. However, using $W_{Stagnation}$ could be used for future oxygenators as a benchmark test to compare new designs with the state-of-the-art devices.

Pulsatility significantly influenced $W_{Stagnation}$. All three pulsatility ratios had a significantly lower $W_{Stagnation}$ compared to the constant flow in each oxygenator. In addition, there were no significant differences between the different pulsatilities. This leads to the assumption that while a 25 % pulsatility ratio yields a better washout, further increase of pulsatility does not lead to improved washout. The observed effect of pulsatility was also shown in Hastings et al., who reported an increased stagnation in clinically used oxygenators driven without a pulse [17]. For $W_{Washout}$ and $W_{Homogeneity,}$ pulsatility had no significant influence. However, a general trend was observable for the parameters. With an increase in pulsatility, $W_{Washout}$ decreases and $W_{Homogeneity}$ increases.

The comparison between different oxygenator designs showed that the two wound oxygenators, Hilite 800 and 2400, had a better washout than the stacked oxygenators, ILA and QSA, quantified by the lower $W_{Washout}$ values. An opposite observation was made regarding flow distribution – the values of $W_{Homogeneity}$ indicated a more homogeneous flow distribution within the two stacked oxygenators. The better performance in flow distribution of the two stacked oxygenators is connected to the lower pressure drop compared to the wound ones [26–28]. Therefore, the blood requires less energy to be transported across the membrane bundle, with the risk of reduced washout, both indicated by differences in $W_{Washout}$ and $W_{Homogeneity}$. In consequence, a clear decision whether wound or stacked fiber bundles are superior regarding washout characteristics cannot be made because a trade-off between these two parameters exists. However, these metrics should be rather utilized during the design development and optimization stage when the overall fiber bundle type is fixed. The washout and blood-flow paths of the whole oxygenator can be optimized by visualizing the washout parameters. Fig. 4 shows the stagnation volume at a volume flow of 1 L/min and a pulsatility index of 75 %. A relationship between the blood flow path and the stagnation volume is evident, with increased stagnation volume as the blood passes farther from the primary inflow and outflow paths. The absence of stagnation in the Hilite 2400 indicates that oxygenator designs have superior operational ranges. In future work, additional flow settings, the impact of pulse frequency and other oxygenators should be investigated to further examine the overall washout behavior.

The study presented here was limited by the numerical methods in treating the fiber bundle as a porous medium, leading to unavoidable simplifications of the flow field. However, the porosity and permeability of the fiber bundle were adjusted according to in-vitro measurements of the individual devices. Although there are approaches that look on the micro-scale flow dynamics across individual fibers [29] or small parts of the fiber bundle, a translation to the full-scale device is still missing. Further on, the multi-phase behavior of blood was not considered, although it does exhibit complex flow physics on the fiber level [30]. The use of the Hilite 800 at two flow rates outside of the recommended flow range (1 L/min and 1.5 L/min) is a further limitation of the study. Thus, the results for the Hilite 800 should be interpreted with caution. The used oxygenators are designed for different flow ranges, which could limit an overall comparison, for instance, between the stacked and wound fiber configurations. In future studies, additional oxygenators should be analyzed to verify the identified differences. However, it has to be noted that off-label use is not uncommon in clinical practice [11] and devices are used outside of their initially intended flow ranges. Thus, the investigated scenarios do occur in the clinics.

Nevertheless, our approach of dimensionless parameters can be applied to more realistic CFD simulations as long as there is a marker to determine velocities and washout behavior of the device.

At last, the oxygenators were reverse-engineered, which could lead to uncertainties in the flow calculations due to deviations of the geometry caused by measurement errors and manufacturing tolerances of the oxygenators.

Furthermore, quantitative validation of the washout parameters is extremely difficult. The study by Kaesler et al. [22] showed a similar velocity pattern for a simplified oxygenator, measured with particle image velocimetry, and a comparable in silico model in a similar flow field. Therefore, we assume the plausibility of the data presented herein. Furthermore, in previous work [31], we have performed CT-scans of contrast media washout in an in-vitro setup using water. Even in such idealized conditions, only a qualitative comparison of CFD simulations and experiments was possible. The performed verification experiment compared the measured and simulated washout time with 99 % washout of blood old. The maximum difference in percentage is 15 %, with only 1 s difference for the Hilite 800 at 1 L/min between measurement and simulation. Therefore, we see the verification of our washout model as successful. However, it was not possible to validate the parameters themselves with currently available technology.

Nevertheless, the model provides a better understanding of the flow field through the oxygenator and potential areas where thrombotic events could occur. These areas within clinical oxygenators should be analyzed next and compared with the results of this study to verify them. There exists prior work in the literature like the studies by Zang et al. [10] or Wagner et al. [19] that have investigated clot composition in membrane oxygenators collected after clinical use.

5. Conclusion

Dimensionless parameters to quantify the thrombosis risk induced by the flow path in membrane oxygenators were presented and determined for four commercial devices. Overall, the defined parameters characterize different aspects of flow induced thrombosis risk and are suitable for parameter-based optimization of oxygenator designs towards improved washout characteristics.

Compliance with ethics guidelines

All authors declare that they have no conflict of interest.

This study does not contain any studies with human or animal subjects performed by any of the authors.

Funding

Open access funding is provided by the Open Access Publishing Fund of RWTH Aachen University.

CRediT authorship contribution statement

Jan Heyer: Writing – original draft, Visualization, Validation, Methodology, Formal analysis, Conceptualization. **Sebastian V. Jansen:** Writing – review & editing. **Ulrich Steinseifer:** Writing – review & editing, Supervision, Resources, Project administration. **Felix Hesselmann:** Writing – review & editing, Supervision, Project administration, Conceptualization. **Michael Neidlin:** Writing – review & editing, Supervision, Project administration.

Declaration of competing interest

The authors declare that they have no known competing financial interests or personal relationships that could have appeared to influence the work reported in this paper.

Supplementary materials

Supplementary material associated with this article can be found, in the online version, at doi:10.1016/j.rineng.2025.108817.

Data availability

Data will be made available on request.

References

[1] W.C. Wrisinger, S.L. Thompson, Basics of extracorporeal membrane oxygenation, Surg. Clin. North Am. 102 (1) (2022) 23–35. Nr.S.
[2] F. Villalba, A. Cristina, D.M. McMullan, R.C. Reed, W.L. Chandler, Thrombosis in extracorporeal membrane oxygenation (ECMO) circuits, ASAIO J. (Am. Soc. Artif. Intern. Organs: 1992) 68 (8) (2022) 1083–1092. Nr.S.
[3] J.S. Penk, S. Reddy, A. Polito, M.J. Cisco, C.K. Allan, M. Bembea, T.M. Giglia, H. H. Cheng, R.R. Thiagarajan, H.J. Dalton, Bleeding and thrombosis with pediatric extracorporeal life support: a roadmap for management, research, and the future from the pediatric cardiac intensive care society: part 2, Pediatr. Crit. Care Med. 20 (11) (2019) 1034–1039. Nr.S.
[4] H.J. Dalton, R. Reeder, P. Garcia-Filion, R. Holubkov, R.A. Berg, A. Zuppa, F. W. Moler, T. Shanley, M.M. Pollack, C. Newth, J. Berger, D. Wessel, J. Carcillo, M. Bell, S. Heidemann, K.L. Meert, R. Harrison, A. Doctor, R.F. Tamburro, J. M Dean, T. Jenkins, C. Nicholson, Factors associated with bleeding and thrombosis in children receiving extracorporeal membrane oxygenation, Am. J. Respir. Crit. Care Med. 196 (6) (2017) 762–771. Nr.S.
[5] P. Masi, L. Gouriet, C. Radu, T. Folliguet, A. Fiore, R. Gallet, F. Bagate, M. Dessap, P. Armand, N. de, Immediate clinical complications occurring during membrane change in patients on veno-venous extracorporeal membrane oxygenation, ASAIO J. (Am. Soc. Artif. Intern. Organs: 1992) 71 (2) (2025) 120–127. Nr.S.
[6] X. Fu, Z. Su, Y. Wang, A. Sun, L. Wang, X. Deng, Z. Chen, Y. Fan, Comparison of hemodynamic features and thrombosis risk of membrane oxygenators with different structures: a numerical study, Comput. Biol. Med. 159 (2023) 106907. S.
[7] J.M. Focke, P.-L. Bonke, N. Gendron, T. Call, U. Steinseifer, J. Arens, M. Neidlin, The influence of membrane fiber arrangement on gas exchange in blood oxygenators: a combined numerical and experimental analysis, J. Membr. Sci. 710 (2024) 123147. S.
[8] R. Graefe, R. Borchardt, J. Arens, P. Schlanstein, T. Schmitz-Rode, U. Steinseifer, Improving oxygenator performance using computational simulation and flow field-based parameters, Artif. Organs 34 (11) (2010) 930–936. Nr.S.
[9] P.C. Schlanstein, F. Hesselmann, S.V. Jansen, J. Gemsa, T.A. Kaufmann, M. Klaas, D. Roggenkamp, W. Schröder, T. Schmitz-Rode, U. Steinseifer, J. Arens, Particle image velocimetry used to qualitatively validate computational fluid dynamic simulations in an oxygenator: a proof of concept, Cardiovasc. Eng. Technol. 6 (3) (2015) 340–351. Nr.S.
[10] J. Zhang, T.D.C. Nolan, T. Zhang, B.P. Griffith, Z.J. Wu, Characterization of membrane blood oxygenation devices using computational fluid dynamics, J. Membr. Sci. 288 (1–2) (2007) 268–279. S.
[11] ELSO: Extracorporeal life support: the ELSO red book. 2022.
[12] C.S. Barrett, J.J. Jaggers, E.F Cook, D.A. Graham, S.K. Rajagopal, C.S. Almond, J. D. Seeger, P.T. Rycus, R.R. Thiagarajan, Outcomes of neonates undergoing extracorporeal membrane oxygenation support using centrifugal versus roller blood pumps, Ann. Thorac. Surg. 94 (5) (2012) 1635–1641. Nr.S.
[13] C.P. O'Halloran, R.R. Thiagarajan, V.V. Yarlagadda, R.P. Barbaro, V.G. Nasr, P. Rycus, M. Anders, P.M.A. Alexander, Outcomes of infants supported with extracorporeal membrane oxygenation using centrifugal versus roller pumps: an analysis from the extracorporeal life support organization registry, Pediatr. Crit. Care Med. 20 (12) (2019) 1177–1184. Nr.S.
[14] E. Papadimas, L. Leow, Y.K. Tan, L. Shen, K. Ramanathan, A.M.T.L. Choong, G. MacLaren, Centrifugal and roller pumps in neonatal and pediatric extracorporeal membrane oxygenation: a systematic review and meta-analysis of clinical outcomes, ASAIO J. (Am. Soc. Artif. Intern. Organs: 1992) 68 (3) (2022) 311–317. Nr.S.
[15] L. Schraven, A. Kaesler, C. Flege, R. Kopp, T. Schmitz-Rode, U. Steinseifer, J. Arens, Effects of pulsatile blood flow on oxygenator performance, Artif. Organs 42 (4) (2018) 410–419. Nr.S.
[16] P.C. Schlanstein, A. Limper, F. Hesselmann, T. Schmitz-Rode, U. Steinseifer, J. Arens, Experimental method to determine anisotropic permeability of hollow fiber membrane bundles, J. Membr. Sci. 546 (2018) 70–81. S.
[17] S.M. Hastings, D.N. Ku, S. Wagoner, K.O. Maher, S. Deshpande, Sources of circuit thrombosis in pediatric extracorporeal membrane oxygenation, ASAIO J. (Am. Soc. Artif. Intern. Organs: 1992) 63 (1) (2017) 86–92. Nr.S.
[18] Demarest, C.T., Shoemaker, S.J., Salna, M.P., Chicotka, S.R., Fung, K., Bacchetta, M.D., Antaki, J.F., Cook, K.E.: The time course of clinical oxygenator failure due to clot formation, 2020.
[19] M.S. Wagner, M. Kranz, L. Krenkel, D. Pointner, M. Foltan, M. Lubnow, K. Lehle, Computer based visualization of clot structures in extracorporeal membrane oxygenation and histological clot investigations for understanding thrombosis in membrane lungs, Front. Med. 11 (2024) 1416319. S.
[20] P.D. Ballyk, D.A. Steinman, C.R. Ethier, Simulation of non-Newtonian blood flow in an end-to-side anastomosis, Biorheology 31 (5) (1994) 565–586. Nr.S.
[21] M. Estakhrposhti, S. Hossein, J.J. Xu, M. Gföhler, M. Harasek, Optimizing hollow fiber membrane oxygenators: a multi-objective approach for improved gas exchange and reduced blood damage, J. Membr. Sci. 731 (2025) 124228. S.
[22] A. Kaesler, P.C. Schlanstein, F. Hesselmann, M. Büsen, M. Klaas, D. Roggenkamp, T. Schmitz-Rode, U. Steinseifer, J. Arens, Experimental approach to visualize flow in a stacked hollow fiber bundle of an artificial lung with particle image velocimetry, Artif. Organs 41 (6) (2017) 529–538. Nr.S.
[23] S. Liao, M. Neidlin, Z. Li, B. Simpson, S.D. Gregory, Ventricular flow dynamics with varying LVAD inflow cannula lengths: in-silico evaluation in a multiscale model, J. Biomech. 72 (2018) 106–115. S.
[24] W.-F. Dai, P. Wu, G.-M. Liu, A two-phase flow approach for modeling blood stasis and estimating the thrombosis potential of a ventricular assist device, Int. J. Artif. Organs 44 (7) (2021) 471–480. Nr.S.
[25] S.J. Sonntag, T.A.S. Kaufmann, M.R. Büsen, M. Laumen, F. Gräf, T. Linde, U. Steinseifer, Numerical washout study of a pulsatile total artificial heart, Int. J. Artif. Organs 37 (3) (2014) 241–252. Nr.S.
[26] Fresenius Medical Care: iLA® membranventilator: datasheet, Novalung. 2025.
[27] Fresenius Medical Care: MEDOS HILITE®. 2025.
[28] Gettingte Group: QUADROX-i small adult and adult choose maximum safety: datasheet. 2025.
[29] G. Poletti, D. Ninarello, G. Pennati, Computational analysis of the effects of fiber deformation on the microstructure and permeability of blood oxygenator bundles, Ann. Biomed. Eng. 52 (4) (2024) 1091–1105. Nr.S.
[30] G. Poletti, R.G. Bardón, G. Dubini, G. Pennati, CFD two-phase blood model predicting the hematocrit heterogeneity inside fiber bundles of blood oxygenators, Ann. Biomed. Eng. 53 (2) (2025) 507–519. Nr.S.
[31] K.P. Barbian, T. Lemainque, I. Grunden, R. Iwa, B. Wiegmann, J. Linkhorst, M. Wessling, J. Heyer, U. Steinseifer, M. Neidlin, S.V. Jansen, Tailored 3D lattice microstructures for enhanced functionality in blood-gas exchange, Adv. Sci. (Weinh. Baden-Wurtt. Ger.) 12 (25) (2025) e2501162. Nr.